PAPER

Check for updates

Efficient adsorption and full spectrum photocatalytic degradation of low concentration PPCPs promoted by graphene/TiO₂ nanowires hybrid structure in 3D hydrogel networks†

Yajie Hu,‡ Yanan Yang,‡ Jiejing Zhang, Shengnan Jin and Hong Zheng (ORCID) *

The removal of low concentration PPCPs from water is a challenging issue. A graphene hydrogel with 3D networks shows great potential for accelerating eddy diffusion of low concentration PPCPs. Herein, to further promote its molecular diffusion, a graphene/TiO₂ nanowires (GNW) hybrid structure was implanted into graphene hydrogel. The as-prepared rGO/GNW hydrogel exhibited significantly enhanced adsorption–photocatalytic performance and excellent stability for low concentration ethenzamide, a typical pharmaceutical pollutant in water, under vacuum ultraviolet (VUV), ultraviolet (UV), visible and near-infrared light irradiation. When the initial ethenzamide concentration was 500 ppb and catalyst dosage was 10 mg/150 mL, ethenzamide was completely removed in 3 min and the corresponding photocatalytic apparent rate constant was 2.20 times that by GNW, 4.09 times that by rGO/P25 and 4.31 times that by rGO/NW under VUV irradiation, respectively, and its removal rate attained 99.0% in 120 min and the corresponding photocatalytic apparent rate constant was 2.06 times that by GNW, 3.34 times that by rGO/P25 and 17.42 times that by rGO/NW under UV irradiation, respectively. The GNW hybrid structure in the hydrogel played a vital role in overcoming the mass transfer resistance of low concentration PPCPs. The as-prepared rGO/GNW hydrogel exhibits significant potential for the removal of low concentration PPCPs from water.

1. Introduction

Pharmaceuticals and personal care products (PPCPs) have attracted increasing concern as emerging pollutants since they are frequently detected on the order of ng L^{-1} to μg L^{-1} in the aquatic environments throughout the world and have posed a risk to drinking water.[1–7] Although they will not cause serious harm to the human body in a short time due to their low concentration in the aqueous environments, they can accumulate to attain sufficient concentration level to threaten human health and will cause permanent damage to the reproductive system, nervous system and immune system after a long-term exposure owing to their complex chemical structure, poor biodegradation and natural attenuation, and strong accumulation.[8,9] Therefore, some efficient methods are urgently needed to control and remove them.

Generally, various wastewater treatment technologies such as advanced oxidation technology,[10] activated carbon process,[11] biological treatment technology,[12] UV treatment technology[13] and membrane separation technology[14] are studied to remove PPCPs in water. However, for low concentration PPCPs, they are difficult to be efficiently removed by these conventional treatment technologies since their mass transfer resistance is difficult to be overcome. Photocatalysis is considered as a promising and ideal advanced treatment technology owing to its mild reaction conditions, strong mineralization ability to persistent pollutants without any chemical input or output and no sludge residue.[15–21] While as a versatile semiconductor, TiO₂ photocatalyst has been widely concerned due to its superior photocatalytic activity, excellent photochemical stability, low cost and low toxicity.[22–24] Some efforts also have been tried to overcome the mass transfer resistance of low concentration PPCPs by doping TiO₂ on microporous zeolite,[25] preparing rice-shaped nanoporous TiO₂ (ref. 26) and nanoporous TiO₂ film with exposed {001} facets[27,28] or implanting Pt single atoms on nanoporous TiO₂ film.[29] However, although abundant nanopores can considerably accelerate the eddy diffusion of low concentration PPCPs and atomically implanted noble metal can significantly accelerate molecular diffusion of low

Beijing Key Laboratory of Materials Utilization of Nonmetallic Minerals and Solid Wastes, National Laboratory of Mineral Materials, School of Materials Science and Technology, China University of Geosciences, Beijing 100083, China. E-mail: zhengh@cugb.edu.cn

‡ The first coauthors.

concentration PPCPs, either poor molecular diffusion or high cost of noble metal still limited their practical application.

In recent years, the practical use of rGO-based photocatalysts has attracted great attention.[30–33] Graphene hydrogel with 3D graphene networks shows great potential for accelerating eddy diffusion of low concentration PPCPs due to its convenient mass transfer channels and rich pore structure.[34,35] Moreover, easy recovery from aqueous solution is advantageous to its practical application.[36] So, the rational construction of TiO_2/graphene hydrogels can not only contribute to providing large specific surface area and high porosity, but also promoting the capture of light by active sites due to light refraction–reflection coming from 3D network structure.[37] Furthermore, photogenerated electron–hole pairs of TiO_2 can be efficiently separated owing to excellent electrical conductivity of graphene. Thereby, it is hopeful that both eddy diffusion and molecular diffusion coming from low concentration PPCPs are effectively overcome. In previous study, TiO_2 nanoparticles were chemically bonded to graphene and formed TiO_2 (P25)–graphene hydrogels, which exhibited a significant enhancement in the removal of methylene blue, in comparison with sole P25.[38] However, lower specific surface area and more agglomeration greatly limited eddy diffusion and molecular diffusion coming from low concentration PPCPs.

Herein, to overcome the agglomeration of TiO_2 in hydrogel and form stable TiO_2/graphene hydrogel with larger specific surface area and higher active sites to effectively promote eddy diffusion and molecular diffusion of low concentration PPCPs, graphene/TiO_2 nanowire (GNW) hybrid structure was prepared first and then used to bond to graphene and form reduced graphene/GNW (rGO/GNW) hydrogel. The as-prepared hydrogel exhibited highly efficient adsorption–photocatalytic activity and excellent stability for the removal of low concentration ethenzamide, a typical pharmaceutical pollutant in water, under VUV, UV, visible and near-infrared light irradiation. The GNW hybrid structure in the hydrogel contributed to uniform dispersion of TiO_2 nanowires on graphene and chemical bonding between graphene and TiO_2 nanowires, and played a vital role in promoting eddy diffusion and molecular diffusion of low concentration PPCPs.

2. Experimental section

P25 TiO_2 nanopowders (anatase, purity 99.8%, average crystal size 10–25 nm) were purchased from Shanghai Aladdin Biochemical Technology Co., Ltd. Natural flake graphite powders were obtained from Sinopharm Group Co., Ltd. Ethenzamide (Sigma-Aldrich, purity > 98%) was used. Other chemicals were analytical grade and deionized water was used in all experiments.

2.1 Preparation and characterization of the samples

GO and TiO_2 nanowires (NW) were prepared using the modified Hummers' method[39] and hydrothermal method reported by Pan et al.[40] with a small modification, respectively. Detailed procedures are shown in ESI.† On the basis of optimal ratios of rGO to

TiO_2 (1 : 100) and rGO to GNW (2 : 5) for maximizing the photocatalytic activity (as shown in Fig. S1†), GNW hybrid structure was prepared according to the following method: 10 mg of exfoliated GO was stirred in 30 mL deionized water for 2 h and then 1 g TiO_2 nanowires were added into the dispersed system. After that, 30 mg L-ascorbic acid and 0.031 mL hydrazine hydrate were successively added and maintained at room temperature under stirring for 6 h. The obtained sample was dried at 80 °C. GNW–graphene hydrogel was prepared using simple room-temperature synthesis method. Briefly, 80 mg of exfoliated GO was stirred in 20 mL deionized water for 1 h and then 200 mg of GNW and 0.24 g of L-ascorbic acid were added simultaneously into the dispersed system. 0.25 mL of hydrazine hydrate was added after stirred for 5 min. The mixture was ultrasonicated for 20 min and kept at room temperature for about 8 h. Then the sample was freezing dried after washed by soaking in deionized water for several times and referred as rGO/GNW. The content of the loaded TiO_2 nanowires was 71%. For comparation, P25–graphene hydrogel and TiO_2 nanowires–graphene hydrogel were also prepared using the same method by replacing GNW with P25 and TiO_2 nanowires, and referred as rGO/P25 and rGO/NW, respectively.

The samples were characterized by TEM, FESEM, XRD, Raman, UV-Vis DRS, XPS, BET, FTIR, PL, EIS determination. Detailed test conditions and instrument model can be found in ESI.†

2.2 Adsorption and photocatalytic degradation of low concentration ethenzamide

The adsorption and photocatalytic performance of the as-prepared rGO/GNW for low concentration ethenzamide were evaluated by a series of static experiments under VUV, UV, visible and near-infrared light irradiation. A 0.6 W VUV lamp with main emission at 254 nm and a minor emission at 185 nm (a 15 W lamp with 25 cm length was reserved 1 cm by packing with tinfoil), a 24 W UV lamp with emission at 254 nm, a 75 W metal halide lamp with a cutoff filter ($\lambda > 420$ nm), and a 150 W near-infrared lamp ($\lambda > 780$ nm) were used as VUV, UV, simulative visible and near-infrared light source, respectively. The reaction under VUV irradiation was performed in a cylindrical glass reactor (as shown in Fig. S2†). Air was bumped into the reactor to keep the uniformity of the reactive system and provide enough oxygen. The reactions under UV, simulative visible and near-infrared light irradiation were performed in a 250 mL container controlled at a constant temperature by a circulating water cooling system. In all adsorption and photocatalytic reactions, 10 mg of sample was dispersed into 150 mL ethenzamide solution with initial concentration of 500 ppb. After mixed in the dark for 10 min to establish adsorption–desorption equilibrium, the illumination was initiated. 5 mL of suspension was taken out at selected time interval and centrifuged for 5 min (9000 rpm) to remove the samples for analysis of ethenzamide. The ethenzamide concentration was determined using a high-performance liquid chromatograph (LC-10AD, Shimadzu, Japan) with a UV detector (SPD-10AV) at 230 nm and a Kromasil C18 column for separation.

To examine the stability of the as-prepared rGO/GNW, the adsorption and photocatalytic experiments of ethenzamide were repeated for three times under VUV and UV light irradiation, respectively. After each one, the as-prepared rGO/GNW was separated and directly used for next test.

3. Results and discussion

3.1 Characterization of the samples

As we know, both GO and TiO_2 nanowires are hydrophilic. When TiO_2 nanowires mixed with appropriate amount of GO to directly prepare rGO/NW hydrogel using room-temperature synthesis method, most TiO_2 nanowires sank and separated from graphene instead of forming uniform and stable hydrogel. While TiO_2 nanowires mixed with a small amount of GO in water, the color of TiO_2 nanowires changed from white to light-brown, indicating that GO had a strong-coupling effect with TiO_2 nanowires. Considering the reducing function of ascorbic acid and hydrazine hydrate, the composite was reduced to generate a uniform and stable GNW. Fig. 1a shows the TEM image of GNW. It can be seen that, in comparison with inter-twined and piled TiO_2 nanowires (as shown in Fig. S3†), a large number of TiO_2 nanowires were tiled and interwoven on the ultrathin graphene nanosheets owing to the presence of the ultrathin graphene nanosheets. Moreover, due to the low content of graphene in the GNW, the graphene nanosheet was well unfolded, which is conducive to the dispersion of TiO_2 nanowires. In comparison with TiO_2 nanoparticles, the nanowires have more uniform dispersion on graphene with less agglomeration, resulting in more direct contact between TiO_2 and graphene, and hence further improved electron–hole pairs separation and transportation. Moreover, the adsorbability of GNW could also obviously improve.[40] The rGO/GNW hydrogel can be successfully prepared when GNW mixed with appropriate amount of GO using room-temperature synthesis method (as shown in Fig. S4†). FESEM image of rGO/GNW is shown in Fig. 1d. In comparison with those of pristine rGO hydrogel (Fig. 1b) and rGO/P25 hydrogel (Fig. 1c), rGO/GNW not only kept a smooth surface of the ultrathin graphene nanosheets with a three-dimensional network structure in rGO hydrogel, but also effectively overcome the agglomeration of P25 in rGO/P25.

XRD patterns and Raman spectra of the samples are shown in Fig. 2. From the XRD patterns (Fig. 2a), we can see that the diffraction peak of GO at $2\theta = 10.5°$ disappeared in GNW, rGO, rGO/NW, rGO/GNW and a new wide diffraction peak of rGO appeared in rGO, rGO/NW and rGO/GNW, confirming that elimination of oxygenated functional groups and the existence of strong π–π stacking interactions between the rGO nano-sheets contributing to gelation in these samples.[39] No wide diffraction peak of rGO was observed in GNW, indicating no gelation occurred, which is consistent with the TEM results of GNW. Possible reason was attributed to low content of rGO in GNW. The diffraction peaks of TiO_2 could be clearly observed in GNW and rGO/GNW, indicating that the crystal structure of TiO_2 was not destroyed by the hybrid and gelation processes.
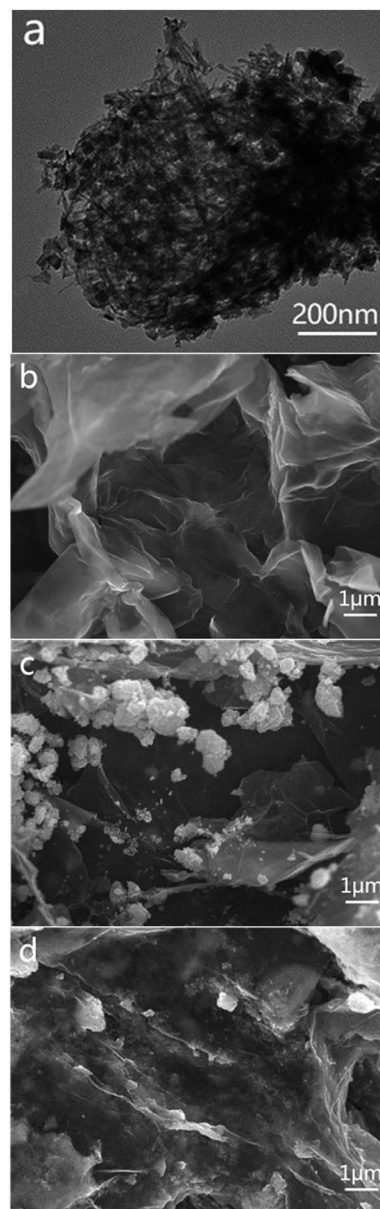

Fig. 1 TEM image of GNW (a) and FESEM images of rGO hydrogels (b), rGO/P25 (c) and rGO/GNW (d).

Raman spectra further provided structural details of the samples. As shown in Fig. 2b, all the samples containing TiO_2 including NW, GNW, rGO/P25, rGO/NW and rGO/GNW revealed the TiO_2 characteristic absorption bands at 149 cm^{-1} (E_{1g}), 396 cm^{-1} (B_{1g}), 516 cm^{-1} (A_{1g}) and 639 cm^{-1} (E_g), confirming the existence of TiO_2. While the D band corresponding to the structural defects or partially disordered graphitic domains and the G band representing tangential C–C stretching vibrations presented in the spectra of all the samples containing graphene.[41] The intensity ratio of the two bands, I_D/I_G, can be used to characterize short-ranged sp^2 carbon moieties and sp^3-hybridized carbon atoms in rGO, thereby, to evaluate the extent of defects/disorder in graphitic structures.[39,41] The higher the number of sp^3 defects/disorder is, the higher the I_D/I_G values
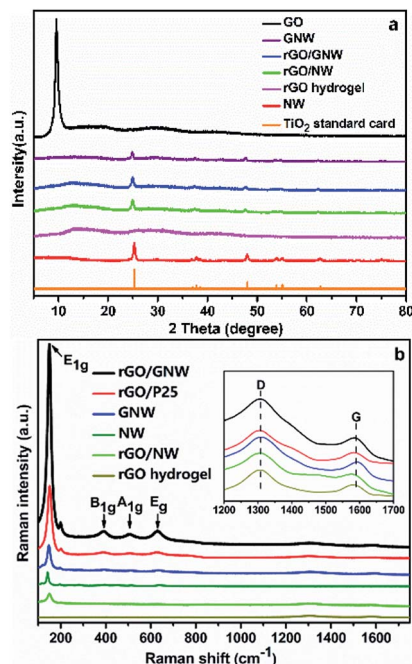
Fig. 2 XRD patterns (a) and Raman spectra (b) of the samples.

are, implying that the smaller the average size of the sp^2 carbon moieties is and hence the higher the degree of GO reduction is. Compared with I_D/I_G ratio of GO (1.9), that of GNW (2.5) increased significantly, indicating that the average size of sp^2 carbon moieties decreased significantly and reduction of GO was significantly increased by the hybrid process. Moreover, in comparison with the I_D/I_G ratios of rGO (2.3), rGO/P25 (3.1) and rGO/NW (3.8), that of rGO/GNW (4.0) also increased significantly, indicating there was a strong interaction between GNW and rGO nanosheets[39] and GNW hybrid structure increased disorder of rGO flakes.

To investigate the effect of GNW hybrid structure on the specific surface area and pore size of the as-prepared hydrogel, adsorption–desorption curves and corresponding pore-size distribution of the samples were determined, the results are shown in Fig. 3. It can be observed that adsorption isotherms of rGO, rGO/P25 and rGO/
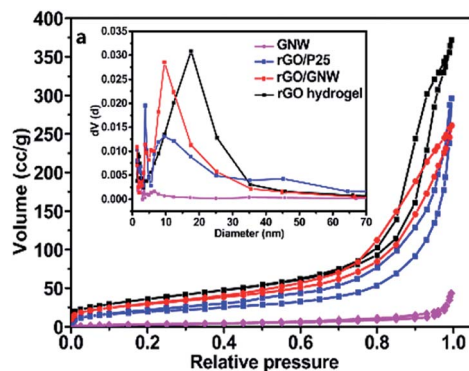
GNW were of IV type isotherms (BDDT classification), suggesting the existence of mesopores (2–50 nm), which is consistent with the results of pore-size distribution in the inset of Fig. 3. Moreover, we can also see that the main pore size of rGO hydrogel was about 17 nm, while those of rGO/P25 and rGO/GNW were about 10 nm and more such pores existed in rGO/GNW, which is consistent with FESEM results. Compared with the specific surface area of rGO/P25 (68 m^2 g^{-1}), that of rGO/GNW (106 m^2 g^{-1}) obviously increased, further confirming that GNW hybrid structure is advantageous for overcoming the agglomeration of TiO$_2$ nanowires although it was slightly lower than that of rGO hydrogel (132 m^2 g^{-1}) due to the inclusion of GNW.

FTIR spectra were used to further examined the functional groups and chemical bond in the samples (Fig. 4). In comparison with GO, the absorption peak intensities of some oxygen-containing functional groups in GNW including epoxy or alkoxy C–O (1045 cm^{-1}), epoxide C–O–C or phenolic C–O–H (1229 cm^{-1}), C=C (1626 cm^{-1}), carboxylate or ketone C=O (1735 cm^{-1}) and water –OH (1626 cm^{-1} and 3415 cm^{-1})[39,42,43] obviously weakened or disappeared, confirming the reduction of GO by hydrazine hydrate and ascorbic acid in the hybrid process. The broad absorption peaks around 400–1000 cm^{-1} in GNW corresponded to Ti–O–Ti and Ti–O–C vibration, confirming the formation of a chemical bond between the rGO and TiO$_2$ nanowires,[44] which is consistent with Raman results. The chemical bond contributed to the dispersion of TiO$_2$ nanowires on the surface of graphene and the formation of stable rGO/GNW hydrogel. The absorption peak intensities of some oxygen-containing functional groups in rGO/GNW and rGO/P25 further weakened or disappeared, confirming that GO was further reduced by hydrazine hydrate and ascorbic acid in the gelation process. The peak at 1569 cm^{-1} in rGO/GNW could be ascribed to the sp^2 hybridization of carbon with adjacent carbon atoms in the graphene sheet and formation of C=C double bond, implying that GNW and rGO were tightly combined by the chemical bond.

To further investigate the surface elemental composition and chemical state of the samples, XPS spectra were determined and are shown in Fig. 5. The presence of Ti, O and C elements in the survey spectra of GNW and rGO/GNW (as shown in Fig. 5a) was consistent with their composition. By fitting the high-resolution spectra of C1s (Fig. 5b), it can be seen that the

Fig. 3 Adsorption–desorption curves and corresponding pore-size distribution (inset) of the samples.
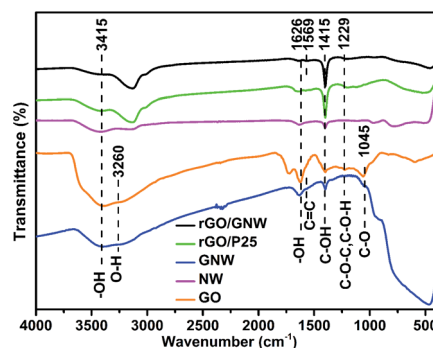

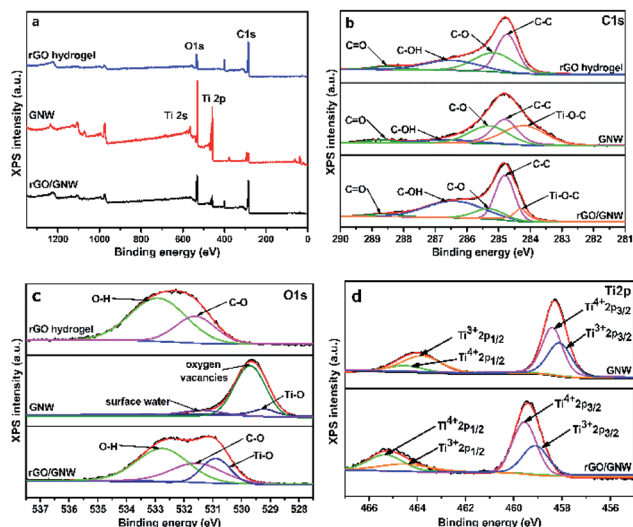Fig. 4 FTIR spectra of the samples.

Fig. 5 (a) Survey spectrum of the sample; (b) C1s; (c) O1s; and (d) Ti2p peaks.

peaks centered at 284.7 eV, 285.1 eV, 286.6 eV and 288.6 eV corresponded to C1s of C–C, C–O, C–OH and C=O in rGO hydrogel, respectively.[45,46] In comparison with C1s of rGO, the presence of Ti–O–C bond in GNW and rGO/GNW further confirmed the formation of chemical bond between TiO_2 nanowires and graphene nanosheets, which contributed to the dispersion of TiO_2 nanowires on the surface of graphene and the formation of stable GNW hybrid structure and rGO/GNW composite. Moreover, the chemical bond could be used as the channel for the efficient transfer of photogenerated carrier.[45] In the high-resolution XPS spectra of O1s (Fig. 5c), O1s in GNW could be divided into three peaks centered at 529.5 eV, 530.5 eV and 531.4 eV, which were assigned to Ti–O bond, oxygen vacancies (O_v) and adsorbed water,[47] respectively. In comparison with GNW, the bonding energies corresponding to the lattice oxygen and O_v in rGO/GNW shifted towards higher binding energy, which was ascribed to the strong interaction between GNW hybrid structure and rGO nanosheets in the process of gelation. The high-resolution spectra of Ti2p (Fig. 5d) could be divided into four peaks corresponding to Ti^{4+} $2p_{1/2}$, Ti^{3+} $2p_{1/2}$, Ti^{4+} $2p_{3/2}$ and Ti^{3+} $2p_{3/2}$, respectively. Similarly, in comparison with GNW, the bonding energies corresponding to Ti^{4+} and Ti^{3+} in rGO/GNW also shifted towards higher binding energy, which was consistent with high-resolution spectra of O1s. On the basis of the high-resolution spectra of O1s and Ti2p, it can be seen that O_v and Ti^{3+} were successfully introduced into GNW and rGO/GNW due to the reduction by reducing agents in the process of hybrid and graphene gelation. Ti^{3+} and O_v could form a new sublevel state at the bottom of the conduction band (CB) of TiO_2 and narrow the band gap of rGO/GNW,[47] which was advantageous to the absorption of long wavelength light. The strong interaction between GNW hybrid structure and rGO nanosheets could accelerate the separation of photogenerated carriers.
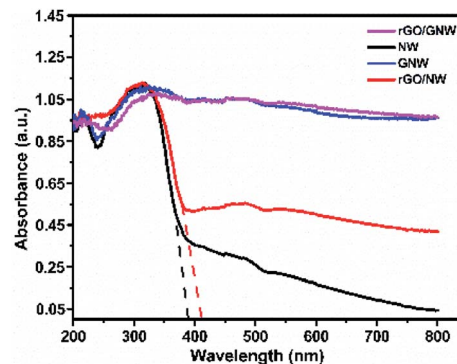

Fig. 6 Diffuse reflectance spectra of different catalysts.

To investigate the light absorption property of rGO/GNW, the UV-Vis DRS spectra of the samples were determined (Fig. 6). Compared with TiO_2 nanowires, the light absorption performance of rGO/GNW was obviously improved. Similar to GNW, light response range of rGO/GNW was expanded to near-infrared region, indicating that the rGO/GNW has potential photocatalytic property in the whole spectrum region. However, in comparison with TiO_2 nanowires, in spite of the absorption spectra of rGO/NW shifted slightly towards long wavelength, much weaker light absorption than rGO/GNW was found. Possible reason was ascribed to the formation of Ti–O–C at the interface between TiO_2 nanowires and rGO in GNW hybrid structure.[48,49]

3.2 Adsorption and full spectrum photocatalytic activity of the as-prepared rGO/GNW

By comparing the adsorption and photocatalytic degradation of ethenzamide by different samples with the same mass, the adsorption and photocatalytic activity of the as-prepared rGO/GNW under VUV, UV, visible and near-infrared light irradiation were evaluated. The experimental results under VUV irradiation are shown in Fig. 7. From Fig. 7a we can see that the adsorption performance of the as-prepared rGO/GNW was significantly improved, adsorption equilibrium was quickly achieved and the equilibrium adsorption rate of ethenzamide reached 21%, which was obviously higher than 15% by rGO/P25, 16% by rGO/NW, 13% by GNW, 10% by NW and 8% by P25, indicating that both 3D network structure of hydrogel and
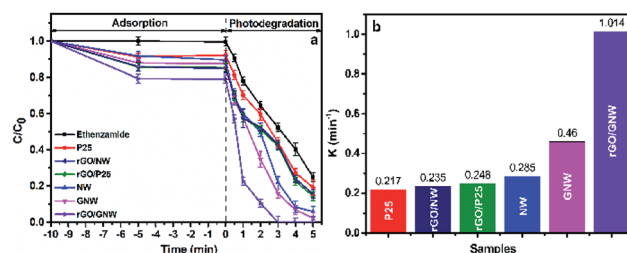

Fig. 7 Adsorption, photocatalytic degradation (a) and corresponding photocatalytic apparent rate constants (b) of ethenzamide under VUV irradiation by the different samples.

GNW hybrid structure are advantageous to adsorption of ethenzamide. The total removal efficiency attained 79% in 1 min, which was also much higher than other samples. The ethenzamide was completely removed in 3 min, which was much faster than other samples. Only one trace intermediate product was observed due to the low concentration of initial ethenzamide. From the corresponding photocatalytic apparent rate constant during the first 2 min (Fig. 7b) it can be seen that, that by the as-prepared rGO/GNW was 2.20 times that by GNW, 3.56 times that by NW, 4.09 times that by rGO/P25, 4.31 times that by rGO/NW and 4.67 times that by P25. The rate constants of the samples were further normalized to the specific surface area (as shown in Fig. S5a†) to evaluate the effect of surface area on the photocatalytic activity. It can be seen that rGO/GNW still showed high value (0.96 min^{-1} m^{-2}), which was 1.85 times that by NW, 2.67 times that by rGO/P25, 2.88 times that by rGO/NW and 2.21 times that by P25. However, GNW showed the highest value (4.1 min^{-1} m^{-2}), indicating the GNW hybrid structure also played a vital role in improving the VUV photocatalytic degradation of ethenzamide by rGO/GNW besides large specific surface area coming from rGO hydrogel.

Fig. 8 shows the experimental results under UV irradiation. Similarly, the equilibrium adsorption rate of ethenzamide by the as-prepared rGO/GNW under the experimental conditions (Fig. 8a) obviously improved and reached 30%, which was far higher than other samples. Different equilibrium adsorption rate from that under VUV irradiation was attributed to different experimental apparatus. After 120 min under UV irradiation, the removal rate of ethenzamide attained 99.0%, which was also much higher than those by other samples. The corresponding UV photocatalytic apparent rate constant during the first 30 min (Fig. 8b) was 2.06 times that by GNW, 1.91 times that by NW, 3.34 times that by rGO/P25, 17.42 times that by rGO/NW and 3.98 times that by P25. Low photocatalytic activity of rGO/NW was ascribed to the separation of TiO$_2$ nanowires from graphene. The rate constant normalized to the specific surface area (Fig. S5b†) also indicated that GNW contributed to UV photocatalytic degradation of ethenzamide. These results further confirmed that both GNW hybrid and 3D network structure of hydrogel play an indispensable role in removing low concentration ethenzamide.

The experimental results under visible and near-infrared light irradiation are shown in Fig. 9. Similarly, the removal rate of ethenzamide by the as-prepared rGO/GNW attained
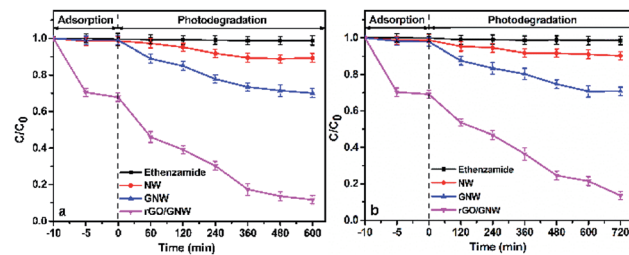

Fig. 9 Adsorption and photocatalytic degradation of ethenzamide under visible (a) and near-infrared light (b) irradiation by the as-prepared rGO/GNW.

87.0% under visible light irradiation for 8 h and 86.2% under near infrared light irradiation for 12 h after adsorption equilibrium, respectively, which was also much higher than those by NW (10.6% and 10.0%, respectively) and GNW (29.9% and 29.1%, respectively). The corresponding visible photocatalytic apparent rate constant during the first 6 h was 4.38 times that by GNW, 17.50 times that by NW and near-infrared photocatalytic apparent rate constant during the first 8 h was 4.00 times that by GNW, 20.00 times that by NW, indicating that the as-prepared rGO/GNW has a good adsorption and full spectrum photocatalytic performance for the removal of low concentration ethenzamide.

To evaluate the stability and reusability of the as-prepared rGO/GNW, the adsorption and photocatalytic degradation of ethenzamide under VUV and UV light irradiation were repeated for three times. Almost no deactivation was found except for 6% decrease of removal rate of ethenzamide under UV light irradiation after 3 recycling uses (Fig. 10), indicating that the as-prepared rGO/GNW has excellent adsorption and photocatalysis stability and can serve as an efficient and stable adsorption and photocatalytic material with full spectrum response for the removal of low concentration ethenzamide.

3.3 Possible adsorption and photocatalytic mechanism of the as-prepared rGO/GNW

PL determination is helpful to understand the separation behavior of photogenerated carriers in the photocatalytic process.[50] Compared with the PL emission peak intensity of NW, those of GNW, rGO, rGO/NW and rGO/GNW successively decreased (Fig. S6a†). On the one hand, the inclusion of rGO
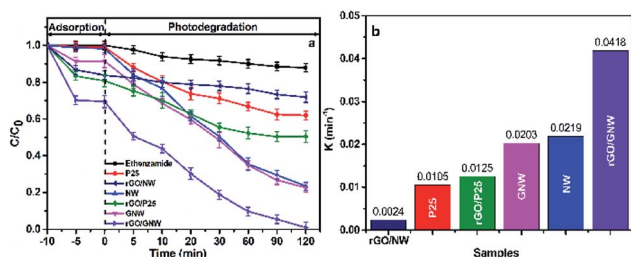

Fig. 8 Adsorption, photocatalytic degradation (a) and corresponding photocatalytic apparent rate constants (b) of ethenzamide under UV irradiation by the different samples.
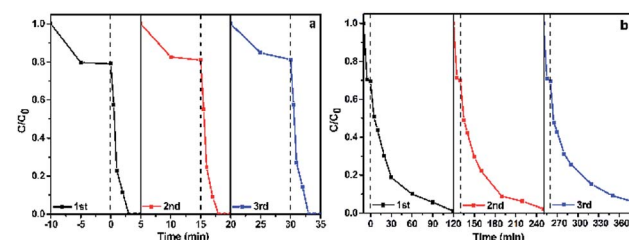

Fig. 10 Cycling runs of the as-prepared rGO/GNW for adsorption and photocatalytic degradation of ethenzamide under VUV (a) and UV (b) light irradiation.

could obviously inhibit the recombination of photogenerated carriers; on the other hand, the three-dimensional framework and interaction of the rGO interfaces could further accelerate the separation of electrons and holes.[38] Moreover, the as-prepared rGO/GNW showed the lowest intensity and almost no PL emission peak was observed, indicating the recombination of photogenerated carriers could be significantly inhibited by the interaction between GNW hybrid structure and rGO hydrogel. EIS results further confirmed the deduction. As shown in Fig. S6b,† the smaller arc radius of the as-prepared rGO/GNW than rGO, NW and GNW further exhibited faster interfacial charge transfer rate in the as-prepared rGO/GNW.[51]

To explicit the active species in the process of photocatalytic reaction, ammonium oxalate, N_2 and *tert*-butyl alcohol (TBA) were used as the capture agents of holes (h^+), superoxide radicals ($\cdot O_2^-$) and hydroxyl radical ($\cdot OH$), respectively and the results are shown in Fig. S7.† It can be seen that the photocatalytic activity of the as-prepared rGO/GNW was significantly inhibited by the addition of ammonium oxalate, N_2 and TBA, especially for ammonium oxalate and TBA, the photocatalytic degradation of ethenzamide almost was completely inhibited. Thereby, it could be inferred that h^+, $\cdot OH$ and $\cdot O_2^-$ played a vital role in the process of the photocatalytic reaction.

On the basis of the above experimental results, a possible adsorption–photocatalysis mechanism for the removal of low concentration ethenzamide by the as-prepared rGO/GNW was proposed, as shown in Fig. 11. Firstly, rGO/GNW hydrogel with 3D graphene networks can contribute to accelerating eddy diffusion of low concentration ethenzamide owing to its convenient mass transfer channels and rich pore structure, thereby, more ethenzamide was adsorbed to active sites of rGO/GNW. Then, TiO_{2-x} with a narrower band gap in rGO/GNW than TiO_2 can be easily excited by light to generate electrons and holes. At the same time, refraction–reflection coming from 3D network structure can promote the capture of light by active sites. Furthermore, photogenerated electrons of TiO_{2-x} in rGO/GNW enter the conduction band of TiO_2 and can smoothly transferred to graphene sheets owing to the higher potential of graphene/graphene$^{\cdot-}$ (-0.08 V *vs.* SHE) than the conduction band position of TiO_2 (-0.24 V *vs.* SHE)[48,52] and favorable channel coming from the chemical bond between NW and

graphene nanosheets, as well as GNW and rGO.[45] The separated electrons can be caught by oxygen molecule adsorbed on the as-prepared rGO/GNW to form $\cdot O_2^-$. $\cdot O_2^-$ can further react with H^+ in the aqueous solution to form H_2O_2 and generate $\cdot OH$.[45] Simultaneously, the holes located in VB can oxide OH^- or adsorbed water molecules to generate $\cdot OH$.[47] As a result, the ethenzamide adsorbed on the surface of rGO/GNW is effectively degraded by these reactive oxidizing species including $\cdot O_2^-$, $\cdot OH$ and h^+. Moreover, oxygen vacancies can promote photocatalytic reaction as catalytic active center. Thereby, molecular diffusion of low concentration PPCPs is effectively promoted.

4. Conclusions

In summary, to promote eddy diffusion and molecular diffusion of low concentration PPCPs in water, rGO/GNW hydrogel was successfully prepared using simple room-temperature synthesis method. The as-prepared rGO/GNW hydrogel exhibited significantly enhanced adsorption–photocatalytic performance and excellent stability for the removal of low concentration ethenzamide from water under VUV, UV, visible and near-infrared light irradiation in comparison with GNW, NW, rGO/P25, rGO/NW and P25.

The GNW hybrid structure in the hydrogel played a vital role in promoting uniform dispersion of TiO_2 nanowires on graphene, chemical bonding between graphene and TiO_2 nanowires, as well as GNW and graphene nanosheets, eddy diffusion and molecular diffusion of low concentration ethenzamide. The as-prepared rGO/GNW hydrogel exhibits significant potential for efficient adsorption and photocatalytic degradation of low concentration PPCPs in water.

Conflicts of interest

There are no conflicts to declare.

Acknowledgements

Fig. 11 Possible adsorption–photocatalysis mechanism of the as-prepared rGO/GNW for the removal of low concentration ethenzamide.

References

1 J. L. Liu and M. H. Wong, *Environ. Int.*, 2013, **59**, 208–224.
2 P. E. Stackelberg, E. T. Furlong, M. T. Meyer, S. D. Zaugg, A. K. Henderson and D. B. Reissman, *Sci. Total Environ.*, 2004, **329**, 99–113.
3 D. J. Lapworth, N. Baran, M. E. Stuart and R. S. Ward, *Environ. Pollut.*, 2012, **163**, 287–303.
4 K. K. Barnes, D. W. Kolpin, E. T. Furlong, S. D. Zaugg, M. T. Meyer and L. B. Barber, *Sci. Total Environ.*, 2008, **402**, 192–200.
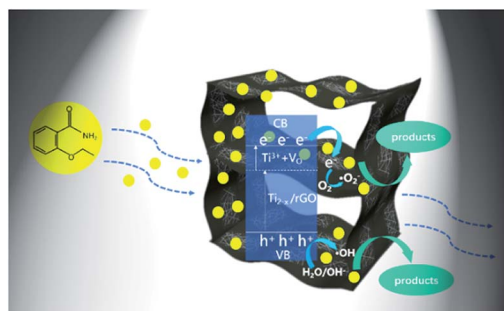
5 M. J. Focazio, D. W. Kolpin, K. K. Barnes, E. T. Furlong, M. T. Meyer, S. D. Zaugg, L. B. Barber and M. E. Thurman, *Sci. Total Environ.*, 2008, **402**, 201–216.

6 R. Loos, G. Locoro, S. Comero, S. Contini, D. Schwesig, F. Werres, P. Balsaa, O. Gans, S. Weiss, L. Blaha, M. Bolchi and B. M. Gawlik, *Water Res.*, 2010, **44**, 4115–4126.

7 M. Stuart, D. Lapworth, E. Crane and A. Hart, *Sci. Total Environ.*, 2012, **416**, 1–21.

8 E. N. Evgenidou, I. K. Konstantinou and D. A. Lambropoulou, *Sci. Total Environ.*, 2015, **505**, 905–926.

9 K. Kuroda, M. Murakami, K. Oguma, Y. Muramatsu, H. Takada and S. Takizawa, *Environ. Sci. Technol.*, 2012, **46**, 1455–1464.

10 D. Vogna, R. Marotta, A. Napolitano, R. Andreozzi and M. d'Ischia, *Water Res.*, 2004, **38**, 414–422.

11 X. Hu, H. Zhang and Z. Sun, *Appl. Surf. Sci.*, 2017, **392**, 332–341.

12 C. Zwiener and F. H. Frimmel, *Sci. Total Environ.*, 2003, **309**, 201–211.

13 I. Kim and H. Tanaka, *Environ. Int.*, 2009, **35**, 793–802.

14 D. L. Nghiem, A. I. Schäfer and M. Elimelech, *Environ. Sci. Technol.*, 2005, **39**, 7698–7705.

15 A. Mills, R. H. Davies and D. Worsley, *Chem. Soc. Rev.*, 1993, **22**, 417–425.

16 M. R. Hoffmann, S. T. Martin, W. Y. Choi and D. W. Bahnemann, *Chem. Rev.*, 1995, **95**, 69–96.

17 V. Vimonses, B. Jin, C. W. K. Chow and C. Saint, *Water Res.*, 2010, **44**, 5385–5397.

18 Y. H. Chiu, T. H. Lai, M. Y. Kuo, P. Y. Hsieh and Y. J. Hsu, *APL Mater.*, 2019, **7**, 080901.

19 M. J. Fang, C. W. Tsao and Y. J. Hsu, *J. Phys. D: Appl. Phys.*, 2020, **53**, 143001.

20 Y. H. Chiu, T. F. Mark Chang, C. Y. Chen, M. Sone and Y. J. Hsu, *Catalysts*, 2019, **9**, 430.

21 D. Awfa, M. Ateia, M. Fujii, M. S. Johnson and C. Yoshimura, *Water Res.*, 2018, **142**, 26–45.

22 Q. Zhang, S. Zhou, S. F. Fu and X. Z. Wang, *NANO*, 2017, **12**, 1750117.

23 Z. Chen, J. Ma, K. Yang, S. Feng, W. Tan, Y. Tao, H. Mao and Y. Kong, *Synth. Met.*, 2017, **213**, 51–57.

24 J. Song, J. Yu, G. Sun, Y. Si and B. Ding, *J. Colloid Interface Sci.*, 2019, **555**, 636–646.

25 Z. Pan, E. A. Stemmler, H. J. Cho, W. Fan, L. A. LeBlanc and H. H. Patterson, *J. Hazard. Mater.*, 2014, **279**, 17–25.

26 F. Sun, W. Zhou, G. Tian, K. Pan, X. Miao, Y. Li, G. Zhang, T. Li and H. Fu, *ChemCatChem*, 2012, **4**, 844–850.

27 T. Xu, H. Zheng, P. Zhang and W. Lin, *RSC Adv.*, 2016, **6**, 95818–95824.

28 T. Xu, H. Zheng, P. Zhang and W. Lin, *J. Mater. Chem. A*, 2015, **3**, 19115–19122.

29 T. Xu, H. Zhao, H. Zheng and P. Zhang, *Chem. Eng. J.*, 2020, **385**, 123832.

30 Y. C. Pu, H. Y. Chou, W. S. Kuo, K. H. Wei and Y. J. Hsu, *Appl. Catal., B*, 2017, **204**, 21–32.

31 K. A. Tsai and Y. J. Hsu, *Appl. Catal., B*, 2015, **164**, 271–278.

32 Y. C. Chen, K. Katsumata, Y. H. Chiu, K. Okada, N. Matsushita and Y. J. Hsu, *Appl. Catal., A*, 2015, **490**, 1–9.

33 Y. S. Chang, P. Y. Hsieh, T. F. Mark Chang, C. Y. Chen, M. Sone and Y. J. Hsu, *J. Mater. Chem. A*, 2020, DOI: 10.1039/d0ta02359k.

34 Y. Wu, J. Zhu and L. Huang, *Carbon*, 2019, **143**, 610–640.

35 Z. Li, T. Chen, S. Liu, M. Zhao, K. Chen, D. Chen and J. Chen, *Catal. Today*, DOI: 10.1016/j.cattod. 2018.07.016.

36 K. He, G. Chen, G. Zeng, A. Chen, Z. Huang, J. Shi, T. Huang, M. Peng and L. Hu, *Appl. Catal., B*, 2018, **228**, 19–28.

37 W. Jiang, W. Luo, R. Zong, W. Yao, Z. Li and Y. Zhu, *Small*, 2016, **12**, 4370–4378.

38 C. Hou, Q. Zhang, Y. Li and H. Wang, *J. Hazard. Mater.*, 2012, **205–206**, 229–235.

39 M. Nawaz, W. Miran, J. Jang and D. S. Lee, *Appl. Catal., B*, 2017, **203**, 85–95.

40 X. Pan, Y. Zhao, S. Liu, C. L. Korzeniewski, S. Wang and Z. Fan, *ACS Appl. Mater. Interfaces*, 2012, **4**, 3944–3950.

41 A. C. Ferrari and J. Robertson, *Phys. Rev. B: Condens. Matter Mater. Phys.*, 2000, **61**, 14095–14107.

42 P. Wang, J. Wang, X. Wang, H. Yu, J. Yu, M. Lei and Y. Wang, *Appl. Catal., B*, 2013, **132–133**, 452–459.

43 Z. Zhang, F. Xiao, Y. Guo, S. Wang and Y. Liu, *ACS Appl. Mater. Interfaces*, 2013, **5**, 2227–2233.

44 Y. Sun, Y. He, B. Tang, Z. Wu, C. Tao, J. Ban, L. Jiang and X. Sun, *RSC Adv.*, 2018, **8**, 31996–32002.

45 L. Xu, L. Yang, E. M. J. Johansson, Y. Wang and P. Jin, *Chem. Eng. J.*, 2018, **350**, 1043–1055.

46 B. Qiu, Y. Zhou, Y. Ma, X. Yang, W. Sheng, M. Xing and J. Zhang, *Sci. Rep.*, 2015, **5**, 8591.

47 X. Liu, Z. Xing, Y. Zhang, Z. Li, X. Wu, S. Tan, X. Yu, Q. Zhu and W. Zhou, *Appl. Catal., B*, 2017, **201**, 119–127.

48 Q. Xiang, J. Yu and M. Taroniec, *Nanoscale*, 2011, **3**, 3670.

49 H. Wu, J. Fan, Y. Yang, E. Liu, X. Hu, Y. Ma, X. Fan and C. Tang, *Russ. J. Phys. Chem. A*, 2015, **89**, 1189–1194.

50 W. Tian, H. Wu, C. Su, Y. Huang, W. Zhao and X. Yang, *J. Photochem. Photobiol., A*, 2018, **350**, 122–129.

51 B. Wu, Y. Li, K. Su, L. Tan, X. Liu, Z. Cui, X. Yang, Y. Liang, Z. Li, S. Zhu, K. W. K. Yeung and S. Wu, *J. Hazard. Mater.*, 2019, **377**, 227–236.

52 W. Wang, J. Yu, Q. Xiang and B. Cheng, *Appl. Catal., B*, 2012, **119–120**, 109–116.